# Shock Structures and Momentum Transfer in Herbig-Haro Jets

Patrick Hartigan
*Rice University*

John Bally, Bo Reipurth and Jon Morse
*University of Colorado*

Herbig-Haro jets record the mass ejection and accretion history of young stars and provide important clues as to how stars form. The use of outflows to constrain the physics of star formation requires an understanding of how shocks within a jet transfer momentum to the ambient medium. Our understanding of how this momentum transfer occurs is improving at a rapid pace driven by (1) spectacular high spatial resolution Hubble Space Telescope images, (2) large format ground-based CCDs with wide fields of view, and (3) velocity-resolved images taken with Fabry-Perot spectrometers and image slicers that enable radial velocities to be measured over a large field of view. HST images of jets resolve the spatial structure of the cooling zones behind the shocks in jets clearly for the first time, and enable us to identify shock fronts and to follow proper motions of subarcsecond structures. Wide field CCDs have shown that outflows from young stars can extend dozens of light years from their sources, which are often multiple systems that drive multiple jets. Velocity and line excitation maps of jets probe the physical conditions within shocked gas, and make possible quantitative comparisons with theoretical models of the flow dynamics. Studies of jets within H II regions are in their infancy, but such objects offer a unique opportunity to observe entire outflows as they are illuminated by ambient ultraviolet light.

## I. INTRODUCTION

Mass loss in the form of winds or jets accompanies newly-formed stars from the time a protostar first appears within a molecular cloud (*e.g.* Bachiller 1996). Millimeter wavelength observations of CO frequently reveal poorly collimated bipolar molecular outflows of low velocity (3 to 30 km $s^{-1}$) in the vicinity of forming stars (*e.g.* Tamura et al. 1996; Moriarty-Schieven et al. 1995). Intermediate velocity ($\sim$ $50 - 100$ km $s^{-1}$) CO 'bullets' are also sometimes observed in bipolar outflows (Cernicharo & Reipurth 1996), and analogous shock-excited emission from infrared lines of $H_2$ are found towards many outflows (*e.g.* Davis & Eislöffel 1995). Along lines of sight that are relatively unobscured by dust, we can observe optical emission line nebulae known as Herbig-Haro (HH) objects. These objects mark the locations where

the highest velocity gas ($> 100$ km s$^{-1}$) cools behind shock waves in the outflow, and often trace a series of bow shocks in highly collimated jets (*e.g.* Reipurth et al. 1997b). Hence, HH objects, near-IR emission from $H_2$, and CO outflows all appear to be manifestations of the mass loss produced during the early stages of the life of a star.

There is growing evidence that strong winds or jets from young stars are powered by unsteady massive disk accretion events (Reipurth 1989; Hartmann et al. 1993). The resulting intermittent outflows produce a chain of internal shocks where faster flow components overtake slower ejecta. Mass outflow rates increase as accretion rates increase (Hartigan et al. 1995), so shocks in jets provide a fossil record of the time evolution of the accretion history of a young star. Where the jet interacts with the ambient medium, it creates external shocks at the ends or the sides of an outflow cavity and accelerates the surrounding gas to produce molecular outflows (*e.g.* Chernin & Masson 1995; Cernicharo & Reipurth 1996).

Outflows appear to play a fundamental role in the process of star formation. In order for a young star to accrete mass, either from spherical infall from the molecular cloud or through a disk, it must lose the angular momentum brought in by the accreting material. Paradoxically, young stars which actively accrete large amounts of material rotate more slowly than their counterparts that do not accrete (Edwards et al. 1993; Bouvier et al. 1993). Hence, accretion disks are able to discard any excess angular momentum very efficiently. As outflow rates are tied to accretion rates, it seems likely that the outflows play a role in removing angular momentum from protostars, without which stars might not form at all except under special initial conditions of almost no angular momentum in the parent molecular cloud core.

HH flows also provide intriguing clues to other unsolved issues in star formation. In several cases, jets have been found to emerge at nearly right angles from a pair of young stars that have projected spatial separations of $< 1500$ AU (Gredel & Reipurth 1993; Reipurth et al., 1993). The presence of a jet around both components of a binary suggests that each star has its own accretion disk, and the lack of alignment means that the rotation axes of the two disks are probably not parallel (jets have been observed to emerge perpendicular to the disk plane; Burrows et al. 1996). An increasing number of Herbig-Haro energy sources appear to be double or multiple systems that reside in exceptionally over-dense regions where interactions between adjacent stars must play a role. Such interactions may be fundamental in determining the symmetries (or lack thereof) of outflows.

Jets may also regulate future star formation within a molecular cloud. The energy deposited into the molecular cloud by outflows from young stars affects the dynamics of the cloud, and may increase turbulence enough to inhibit gravitational collapse of additional protostars.

This feedback of kinetic energy deposited into the cloud by outflows is likely to be most important where jets are common, such as near clusters of young stars.

The recent literature contains a number of articles and even entire volumes devoted to reviews of Herbig-Haro objects (*e.g.* the Chamonix conference proceedings; Reipurth & Bertout 1997), accretion and outflow phenomena (Livio 1997), and shock waves (Draine & McKee 1993). In this chapter we will focus on the most recent developments that are changing the way we look at how young stellar outflows interact with their environment. The closely related topic of how accretion disks collimate infalling material into a supersonic jet is also of great interest to studies of star formation, and is reviewed in the chapters by Eislöffel et al, and by Shu et al.

There have been several major developments in the study of outflows in general and Herbig-Haro objects in particular within the last few years:

• The high angular resolution of HST resolves the transverse extents of stellar jets and the structure of many shocks (Burrows et al. 1996; Heathcote et al. 1996; Ray et al. 1996; Reipurth et al. 1997b; Hester et al. 1998). A key to understanding these images has been to realize that collisionally excited H$\alpha$ from the immediate postshock region marks the location of shocks in the flow, while forbidden line emission follows behind the shock as the gas cools and recombines. Being able to observe where the shock fronts occur within a jet has eliminated much of the speculation that often accompanies interpretation of images. HST has allowed us to measure proper motions on time-scales short compared to the cooling time in the post-shock layer. Therefore, for the first time, we can reliably distinguish between true proper motion and photometric variations in the intensity of the emission from post-shock gas.

• Interactions of the gas within jets and with the surrounding medium are controlled by the flow dynamics, which are revealed to us *via* proper motions, radial velocities, and emission line ratios at each point in the flow. Measuring these quantities across an entire outflow and presenting the information in a comprehensible manner is an major challenge. One of the most useful ways to display kinematic data for a spatially extended object like a jet or HH object is to construct an image of the region at each radial velocity. Within the last few years it has become possible to make velocity images of jets using either a Fabry-Perot spectrometer (Morse et al. 1994) or an image-slicer (Lavalley et al 1997). These data sets provide a powerful means to test any numerical model of collimated outflow quantitatively.

• Because star formation is highly clustered, HH flows also tend to be clustered. For example, the NGC 1333 cloud core shows a "burst" of HH flows emerging from a number of embedded young stars (Bally et al.

1996b). When all of the substructure is taken into account, this single 2 pc diameter region contains several hundred individual shocks, produced by several dozen active outflows from about 100 low mass young stars that have recently formed in this cloud core. A significant fraction of the surface area of the cloud is covered by visible shocks, demonstrating that such shocks, produced by outflows from low mass young stars, must have a profound impact on the surrounding environment, as they burrow cavities through the cloud core, entrain cloud material, and ultimately deposit their energy into the intercloud medium.

• Within the past few years, dozens of *parsec* scale HH flows driven by low mass, pre-main sequence stars have been found in nearby star forming regions (Bally & Devine 1994; Bally et al. 1996a; Bally et al. 1996b; Reipurth et al. 1997a; Eislöffel & Mundt 1997). These flows are up to ten times longer than previously recognized HH flows, and sometimes extend over a degree on the plane of the sky. Giant flows frequently show S-shaped point symmetry, evidence that the orientation of the jets changes on time scales shorter than the time required to accrete the mass of the star (Gomez et al. 1997).

• Finally, any high velocity gas within an H II region will become visible as it is ionized by the ambient ultraviolet radiation. Within large H II regions like the Orion Nebula, it is difficult to separate high velocity material from the bright stationary nebular gas, but this separation can be accomplished with Fabry-Perot spectroscopy (O'Dell et al. 1997a). Jets may also become ionized locally in the immediate vicinity of the young O and B stars that drive them. These jets are frequently one-sided and are powered by sources which suffer relatively low obscuration. Such irradiated jets provide a new way to investigate the wind formation and jet collimation mechanisms, because with these systems we observe the entire outflow, not just the portion that radiates behind a shock (Reipurth et al. 1998a).

In this chapter we shall consider each of the new developments listed above, particularly how they relate to jet propagation, and momentum transfer. Emission lines from shocks provide the principal means by which we can study stellar jets; we consider the physics of these radiative shocks and measures of mass loss rates in section II. The momentum transfer within jets as defined by morphologies, radial velocities, and proper motions of the shocks is covered in section III, with a brief discussion of molecular emission in section IV. Large-scale HH flows are discussed in section V, multiple jets in section VI, and externally ionized jets in section VII.

## II. EMISSION LINE DIAGNOSTICS OF HH SHOCKS

Because it is possible to measure radial velocities and emission line ratios at any position within an HH flow that radiates, we can

determine the physical conditions throughout these flows directly. Such observations give powerful constraints on models of jets, but because HH objects often emit dozens of lines at optical wavelengths, each with a resolved velocity profile that varies spatially across the object, it is easy to become overwhelmed by the sheer volume of information. In this section we will consider how to interpret spectra of HH objects, and explore what these data tell us about conditions in the flows.

### A. Structure of Radiative Shocks

The high radial velocities and similarity of HH spectra to those of supernovae remnants prompted Schwartz (1975) to propose that HH objects were radiative shocks. Astronomers call a shock 'radiative' if it cools by emitting radiation on a timescale short compared with cooling by adiabatic expansion. Examples of *non*-radiative shocks include some supernovae remnants, where the gas behind the shock is too hot and rarefied to radiate emission lines efficiently, so the shock is detectable only through radiation of X-ray and radio continuum or lines of H excited by collisional excitation immediately at the shock (Chevalier et al. 1980).

The basic structure of a radiative shock is shown in Fig. 1. Within the frame of reference of the shock, considered here as an infinitesimally thin interface, preshock material enters from the left with a density $n_0$ at a velocity V, known as the shock velocity. Because $V > C_S$, the sound speed in the preshock gas, the postshock material to the right of the shock is unable to communicate to the preshock gas *via* sound waves that the preshock gas is about to encounter a denser, slower portion of the flow. As a result, the preshock gas suddenly undergoes a jump in density and temperature, known as a J-shock. By balancing momentum, energy, and mass across the shock one can derive the Rankine-Hugoniot jump conditions (Zel'dovich & Razier 1966), which show that strong shocks (those with high Mach numbers $M = V/C_S$) in atomic gas undergo an increase in density by a factor of 4 across the shock. Because the mass flux $\rho v$ is conserved across the shock, the postshock velocity drops to V/4 with respect to the shock front. Most of the kinetic energy of the preshock gas for high Mach number shocks goes into heat; the postshock temperature is proportional to $V^2$. Incident ions carry more kinetic energy than the electrons do, so at the shock the ion temperature initially exceeds the electron temperature, but the two temperatures later equilibrate owing to Coulomb collisions.

Several processes can modify the simple picture described above. Though the supersonic speed of the preshock gas prevents it from encountering any sound waves from the postshock gas, the postshock gas *can* affect the preshock gas through various processes called precursors. One of the most important of these is a radiative precursor, where ultraviolet emission from the hot postshock gas emerges from the shock

and ionizes the preshock gas (Sutherland et al. 1993; Dopita 1995; Morse et al. 1996). When ionized preshock gas enters the shock, energy that would have gone into ionizing the gas now goes into increasing the postshock temperature. Hence, emission from a preionized shock resembles that from a higher velocity neutral shock (Cox & Raymond 1985). In the absence of an external illuminating source, the transition from neutral to preionized shocks occurs around 100 km $s^{-1}$ (Shull & McKee 1979; Hartigan et al. 1987).

Magnetic precursors may be particularly important in molecular shocks. In this case magnetic waves propagate ahead of the shock and excite any ions in the preshock gas, which then collide with and gradually heat the neutral molecular component before it encounters the shock. When the field is very strong it may eliminate the J-shock altogether and leave a smooth increase of temperature and density known as a C-shock (Draine 1980; Draine & McKee 1993; Hollenbach 1997). Magnetic fields also influence the physics at the shock by redirecting the highest energy ions back into the preshock gas. This process is thought to generate cosmic rays, and may produce a precursor that heats the preshock gas, but this effect has not been explored in any detail for HH objects. Finally, some of the energy that would go into heating the gas at the shock compresses the magnetic field instead, so magnetic fields reduce the postshock temperature to levels expected from a lower velocity, nonmagnetic shock.

Thus far we have discussed only the physics at the shock front. Immediately behind the shock any neutral H suddenly encounters a very hot environment. For a wide range of energies there is a 10% – 20% chance that a H atom will become collisionally excited before it is ionized (Chevalier & Raymond 1978; Chevalier et al 1980; Hartigan 1997). *This process is extremely important for HH shocks, because it implies that strong, sharp H$\alpha$ features in emission line images denote the positions of shock fronts in the outflows.*

As the gas radiates emission lines it gradually cools and recombines. Species such as O III are followed by O II and finally O I in well-defined cooling zones behind the shock (Raymond 1979; Fig. 1). These cooling zones are nowhere near ionization equilibrium, so to predict emission line fluxes and ionization fractions accurately one must construct a numerical code that follows the time-dependence of the cooling in each line of interest. Forbidden lines such as [O I] $\lambda$6300, [N II] $\lambda$6583 and [S II] $\lambda$6731 are excited by hot electrons in the postshock gas.

The gas in HH objects is largely transparent to optical photons, but radiative transfer can be important at ultraviolet wavelengths. When the postshock gas cools below $\sim 10^4$K it usually becomes opaque to Lyman continuum photons, and ultraviolet resonance lines are scattered in some cases (Hartigan et al. 1998). If enough ultraviolet light is present near the shock this energy can propagate downstream and

reionize a sizable fraction of the gas after it recombines. All numerical codes must account for these radiative processes, which affect the observed line fluxes. Fortunately, the physics of ionization and collisional excitation is understood well, and different numerical codes give about the same answers when applied to identical test problems (Ferland et al. 1995). Abundances within HH objects appear to be close to solar, without any significant depletion of refractory elements onto grains (Hartigan et al. 1998; Beck-Winchatz et al. 1996).

### B. Measures of Shock Velocities, Densities, and Magnetic Fields in HH Objects

The most important parameters that control the physics of the line emission from HH objects are the geometry and velocity of the shock, the preshock density, and possibly the magnetic field. In practice, observed fluxes, line widths, and images are combined with emission line ratios to estimate the shock parameters. Line ratios alone indicate electron densities and temperatures within HH objects as they do in other emission nebulae, but it is not always straightforward to interpret these because the gas emits over a range of densities and temperatures behind a radiative shock.

The following describes the procedure that one typically follows to model an HH object. The best way to get an overview of the object is to investigate emission line images and attempt to identify the location and shape of the shocks present. As described above, sharp Balmer emission outlines the locations of shocks except for high shock velocities, where the preshock gas is ionized and it is easy to identify the shocks *via* high-excitation lines. Low-excitation lines like those from O I and S II should follow in the cooling zone behind the shock, typically $100 - 1000$ AU for most HH objects. If the shock is curved like a bow, the highest excitation lines like [O III] $\lambda 5007$ should occur near the apex of the bow. In fact, because [O III] lines only occur when the shock velocity exceeds $\sim 90 - 100$ km s$^{-1}$, the point where [O III] emission vanishes along the bow indicates that the velocity of material across the shock has decreased to $\sim 100$ km s$^{-1}$ at that point.

The above information, together with the observed shape of the bow shock, gives a measure of the shock velocity (*e.g.* Morse et al. 1992). Another measure of the shock velocity for a bow shock are the widths of the emission lines, which equal the shock velocity for any emission line that emits over the entire bow shock independent of the viewing angle and preshock density (Hartigan et al. 1987). Line widths are good diagnostics of the shock velocity provided that thermal or magnetic broadening is small compared with the shock velocity, as is the case for most emission lines except perhaps for the collisional component of the Balmer lines, which emits at a high temperature immediately behind the shock and can broaden H emission line profiles

(*e.g.* Morse et al. 1993).

Proper motions and radial velocities indicate the orientation angle of the flow, and this information is also contained within the emission line profiles (Heathcote & Reipurth 1992; Hartigan et al. 1987). The shock velocities implied by the emission line widths and line ratios are significantly lower than the space velocities measured by radial velocities and proper motions. Hence, HH objects move into material that already moves away from the young star at hundreds of km $s^{-1}$. For this reason, shocks that are strong enough to generate [O III] are fairly rare in HH objects, and occur only in the brightest bow shocks that also have large line widths.

One of the best diagnostics of the preshock density is the total observed flux of a bright line like H$\alpha$. While the volume emission coefficient $\epsilon$ (erg $cm^{-3}$ $s^{-1}$) typically scales as $N^2$, where N is the density, sizes of cooling zones behind shocks are proportional to $N^{-1}$, so the fluxes F of most lines tend to scale linearly with N. This dependence makes sense when we consider that a certain number of photons are emitted for each atom that crosses the shock, so doubling the preshock density tends to make most lines twice as bright. The dependence is not exact for each line however, because the densities may exceed the critical densities for some lines and induce collisional quenching. For these lines, $\epsilon \sim N$, and $F \sim$ constant. Even though the preshock density may be in the low density limit for a given transition, the postshock density may increase past the high density limit as the gas cools and compresses.

Both line fluxes and line ratios need to be dereddened, and for HH objects this correction is not always easy because H$\alpha$/H$\beta$ ratios in low velocity shocks typically range as high as $5-6$, much larger than their recombination value of about 3 (Osterbrock 1989). The intrinsic Balmer decrement can only be assumed to be $\sim 3$ in high-excitation HH objects where the Balmer emission from collisional excitation at the shock contributes negligibly to the total flux. When an H II region exists nearby, the Balmer decrement there gives a reddening. Other combinations of HH emission lines are sometimes used to estimate reddenings, but these are either inaccurate (in the case of comparing emission from different atoms), or difficult to measure (such as lines that originate from the same upper level, like the blue [S II] doublet and the [S II] lines around 1$\mu$m). If UV observations are available, one can use the shape of the 2-photon continuum to estimate a reddening (Hartigan et al. 1998).

The magnetic field B is probably the most difficult parameter to estimate because emission lines from a shock with a strong magnetic field resemble those from a lower velocity nonmagnetic shock (Hartigan et al. 1994). However, if one has already measured the shock velocity and density by the methods described above, it is possible to estimate

the component of the magnetic field along the shock by comparing the density in the [S II] emitting region with that expected if no magnetic fields were present. Because B is proportional to N, the magnetic field in the cooling zone increases as the postshock gas cools and compresses, so the magnetic pressure $B^2/8\pi$ also increases. The additional magnetic pressure from even a weakly magnetized shock can reduce the density in the [S II] emitting region by an order of magnitude compared with an identical nonmagnetic shock. For this reason any secondary shocks within the cooling zone should be strongly magnetized (Hartigan et al. 1998). When applied to bow shocks, which are typically 0.1 pc from their exciting stars, these methods have given preshock magnetic fields of $30\mu$G – $100\mu$G (Morse et al. 1992; 1993; 1994), similar to estimates of the magnetic field within dark clouds (*e.g.*, Heiles et al. 1993).

Not all predictions of emission lines from shock models are equally reliable. For example, the Ca II infrared triplet at 8500Å is difficult to model correctly because the fluxes in these lines depend upon the amount of resonant scattering in the H and K lines which pump the 4p level. Similarly, the fluxes from C I are difficult to quantify because molecules may become important coolants at low temperatures.

### C. Mass Loss Rates

We would like to be able to measure the mass loss rates within jets as accurately as possible because the ratio of mass accretion to mass outflow rates is one of the parameters predicted by theories of jet formation and collimation (*e.g.* Najita & Shu 1994). Unfortunately, while most methods applied to a group of jets can sort the mass loss rates from highest to lowest, no method can claim to be accurate to better than a factor of 3 – 10.

Because we can measure the cross-sectional area $A$ of most jets, as well as the velocity $v$ and density $\rho$, it is not hard to calculate $\rho v A$, which is the mass loss rate. The first difficulty with this method is that what is actually measured from the emission line ratios is the electron density $N_e$. To convert $N_e$ to the total density N we must divide by the ionization fraction X of the gas where the emission line is measured. The ionization fraction in the [S II] emitting region (where $N_e$ is measured) is typically 3% or so in the best shock models (Hartigan et al. 1994), though some analytical approximations give values closer to 10% (Raga 1991).

The main difficulty now becomes how to interpret this mass loss rate. Within the frame of reference of the shock, the velocity is inversely proportional to the density, so it does not matter where we measure $\rho v$. However, in a stellar jet the shock itself moves outward at a velocity close to that of the flow speed. Because the gas is compressed behind the shock, the mass loss rate appears much higher there than it does in front of the shock. This inherent clumpy nature of an outflow creates

uncertainty in mass loss estimates. One procedure is to correct for the compression produced by the shock to estimate an 'average' mass loss rate in the jet (Hartigan et al. 1994).

Other methods commonly used to estimate mass loss rates depend upon the total luminosity in a particular emission line. One procedure assumes that the dominant coolant below about 5000 K for any atomic shock is the [O I] 63$\mu$m line (Hollenbach 1985). Hence, one can relate the luminosity $L_{[OI]63\mu m}$ directly to the mass loss rate by $L_{63\mu m} = 3kT\dot{M}/(2\mu m_H)$, where k is Boltzmann's constant, T is the temperature where the line emits, $m_H$ is the mass of the hydrogen atom, $\mu$ is the mean molecular weight, $\dot{M}$ is the mass loss rate. An analogous expression can be derived for other emission lines by introducing a constant $f$ to the right side of the equation, or by calculating the number of photons of a particular line that are emitted for each atom that crosses the shock (see Hartigan et al. 1995 for a discussion). The trouble with all these methods is that stellar jets typically have multiple shocks along the jet, and each of these shocks generates its own cooling zone and line emission. Hence, these methods tend to overestimate mass loss rates because each atom in the jet may pass through many shocks as it moves away from the star.

Another approach is to simply add up all the emission observed within a given aperture, and convert this to a total mass assuming standard abundance ratios. Measures of the velocity then give the mass loss rate. The drawback with this method is that not all of the gas within the flow radiates – we observe only the portion that has been heated recently by a shock. Moreover, no single emission line traces both the hottest and coolest regions behind a radiative shock. In this regard, study of jets within H II regions may prove useful because with sufficiently strong ambient ultraviolet radiation we can be assured of seeing all of the high velocity gas (see section VII).

## III. MOMENTUM TRANSFER WITHIN STELLAR JETS

### A. Bow Shocks and H$\alpha$ Arcs Within Jets

The first indication that HH flows transfer momentum along their axes *via* bow shocks came from observations of large emission line widths of up to 200 km $s^{-1}$ in many objects (Schwartz 1981). Bow shocks are a natural explanation for large linewidths in small objects because material is pushed away from the axis of the flow as it enters the bow. Triangular position-velocity diagrams and double-peaked emission line profiles characteristic of bow shocks were subsequently observed in a number of objects (Solf et al. 1986; Hartigan et al. 1987).

As more HH objects were imaged over larger fields of view, several clear examples of bows emerged, many lying along the axis of narrower

collimated jets. It was initially thought that stellar jets may transfer momentum to their surroundings in an analogous manner to what was seen in numerical models of extragalactic jets (Norman et al. 1982; Cioffi & Blondin 1992), where large, hot backflowing cocoons may excite internal shocks along the jet. However, no kinematic evidence exists for the backflowing cocoon in stellar jets, or for an extended region of million degree gas surrounding the jet. The most important differences between stellar and extragalactic jets seem to be that stellar jets are denser than extragalactic jets, and therefore cool radiatively and do not form hot cocoons. Also, stellar jets are much denser than their surroundings, and essentially plow through the interstellar medium as a series of bullet-like objects (*e.g.* Reipurth et al. 1997b).

When two fluids collide supersonically, a shock should propagate into each fluid. In the case of HH objects, the 'forward' shock which accelerates the slower material is the bow shock, and the 'reverse' shock which slows the faster gas closer to the star is the Mach disk. The Mach disk is probably a time-variable structure and may be subject to a number of instabilities (Blondin et al. 1990; Stone & Norman 1993). Theoretically, both Mach disks and bow shocks should be radiative (Hartigan 1989), and both shocks have been successfully identified in a number of objects both *via* their distinctively different line ratios and by their differing kinematics (Morse et al. 1992; Reipurth & Heathcote 1992). In most cases the bow shock has a higher shock velocity than does the Mach disk, indicating that the jet is denser than the medium into which it propagates.

Though the emission line widths are larger and more high-excitation lines exist in spectra of bright bow shocks in HH flows than occur within jets, neither the line widths nor the line excitations are as high as they should be if the bow shocks accelerate stationary gas. This fact, together with images of multiple bow shocks, led to the idea that HH flows consist of a series of nested bow shocks. Such systems have now been imaged with great clarity with HST (Burrows et al. 1996; Heathcote et al. 1996; Ray et al. 1996; Reipurth et al. 1997b; Hester et al. 1998), and also show the kinematics expected for dense flows moving into the wakes of previous mass ejections (Hartigan et al 1990; Morse et al. 1994).

The transfer of momentum from the jet laterally is of great interest because this process may drive molecular outflows. Jets were found to have higher radial velocities along their axes than they have at their edges, which led to the idea that material is entrained in a turbulent manner along the edges of jets and along bow shocks (Solf 1987; Raga & Cabrit 1993; Raymond et al. 1994; see Hartigan et al 1996 for a discussion). However, a series of bow shocks would also set up a velocity field with the highest velocities along the axis of the flow. To distinguish between the two models, one must look to the shock

velocities, which should be highest along the apex for bow shocks, but highest in a mixing layer at the edge of the jet for entrainment. When ground-based images showed the highest H$\alpha$/[S II] line ratios occurred along the edges of the flow, it seemed as if entrainment produced much of the observable emission in HH objects because this ratio increases with shock velocity (Hartigan et al. 1993).

However, new HST images of jets show that H$\alpha$ is remarkably sharp spatially, not at all like a cooling zone behind a fast, turbulent shock. The morphology of these H$\alpha$ arcs (Fig. 2) appear exactly like the wings of bow shocks, though sometimes these arcs appear only along one side of the jet, as if the flow axis varies with time (see section V). Strong H$\alpha$ occurs in the HST images because this emission is concentrated near the shock front, while the [S II] emission is more extended spatially within the cooling zone behind the shock. At the edges of the HH 111 jet, the H$\alpha$ arcs suddenly become fainter at a distance of about 200 AU from the axis of the jet, as would occur if the preshock density of the medium which surrounds the jet is much lower than that within the jet (Fig. 2). Hence, this ambient medium plays no significant role in keeping the jet collimated, in agreement with images which show that jets are collimated within a few hundred AU from their driving stars (Burrows et al. 1996; Ray et al. 1996).

While 'prompt' entrainment (where material is pushed ahead by a series of shock waves; DeYoung 1986) dominates the dynamics of most HH flows, at least one object exists where turbulent entrainment appears to be important. The HH 110 outflow appears as a diffuse, curving outflow in emission line images (Reipurth & Olberg 1991; Raga et al. 1995; Noriega-Crespo et al. 1996). Attempts to identify the exciting source for this flow failed until it was realized that the flow arises from a highly collimated jet that has undergone a complete change of direction after impacting the edge of a dense molecular cloud (Reipurth et al. 1996). The interface between the molecular cloud and the redirected jet appears quite irregular, and shocks appear in both the HH flow and within the molecular cloud. This region is probably the best example to date of a turbulent HH flow. Younger HH flows that are obscured optically and become visible through shocked $H_2$ emission are other places to look for turbulent entrainment (Davis & Smith 1996b; section IV).

### B. Radial Velocity and Excitation Maps of HH Flows

Together with the proper motions discussed in the next section, radial velocities show how the gas moves within HH flows. In the case of a single bow shock, material is pushed ahead at the highest velocity at the apex of the bow. However, this position will only be the highest radial velocity if the bow moves directly toward or away from us. In the limit where the bow moves in the plane of the sky, the radial velocity

at the apex will be zero, and the largest radial velocities, both positive and negative, will be displaced away from the apex along the axis of the bow. Many papers have explored how velocities should vary with position along a long slit for a bow shock (Raga & Böhm 1986; Solf et al. 1986; Hartigan et al. 1990). For most viewing angles, larger linewidths occur near the apex of a bow than appear in the wings.

As discussed above, shocks with markedly differing velocities, like a bow shock and Mach disk, can often be identified with relative ease by comparing two emission line images, such as H$\alpha$ and [S II]. The spatial structure of a bow shock should also show excitation gradients, with the highest ionization lines occurring at the apex of the bow. Such gradients are observed (*e.g.* HH 34 Morse et al. 1992; HH 1 Hester et al. 1998), where high ionization lines like [O III] $\lambda$5007 emit only near the apices of bow shocks.

Within the last few years, it has become possible to measure radial velocities over entire HH flows with Fabry-Perot spectrometers (*e.g.* Morse et al. 1992) and image slicers (Lavalley et al. 1997). A combination of radial velocities, proper motions, line profiles and line excitations gives a large set of constraints that any theoretical model must satisfy. An example of the remarkable power of such observations is shown in Fig. 3, where the velocity field of the L 1551 jet shows clearly that the bright knot at the end of the jet is a bow shock, with large linewidths near the apex, and slower gas along the edges. In contrast, the kinematics around HH 29 in the same outflow is much more complex, and shows several bright knots with large linewidths contained within a larger curved structure. In HH 29 it appears that the large, curved bowshock seen in H$\alpha$ has wrapped around these slower, dense clumps in the flow seen in [S II] (see also Fridlund et al 1998). This interpretation predicts that the knots marked in Fig. 3 should have relatively slower proper motions, larger linewidths, and higher excitations as compared with adjacent bow shock gas, as is observed.

### C. Proper Motions in Jets

Herbig-Haro objects represent one of the few classes of a spatially extended astronomical object where both structural changes and proper motions can be measured with relative ease. The HH 29 region described above is a striking example of a shock whose morphology changes dramatically within a year or two in response to the transfer of momentum from a powerful outflow to its surroundings. Proper motions for the closest HH objects like HH 29 become apparent in ground-based images within a few years, but the interval is reduced to less than a year with the superb $0.05''$ to $0.1''$ angular resolution of the Hubble Space Telescope. Though proper motions of HH objects have been measured since the early 1980s (*e.g.* Herbig & Jones 1981), it is only with the high angular resolution of HST that we can begin

to distinguish true proper motions from photometric variations in the intensity of emitting gas within the post-shock cooling zone.

The wide field of view of modern CCDs also provides the first opportunity to determine the proper motions of entire parsec-scale outflows (Devine et al. 1997; Reipurth et al. 1997a). When combined with three-dimensional spectroscopic mapping of the radial velocity fields of the associated shock systems of entire outflows, proper motions will enable us to diagnose the full spatial and velocity structure of outflows in 5 of the 6 phase-space dimensions.

Several general conclusions can be drawn from recent results of proper motion studies:

(1) Photometric variations are more apparent in H$\alpha$ than they are in [S II]. This difference makes sense when we consider that most of the H$\alpha$ emission from low-velocity shocks comes from collisional excitation in the immediate vicinity of the shock front. Hence, any sudden increase in the preshock density, such as would occur in a clumpy flow, would produce a corresponding increase in the H$\alpha$ intensity. In contrast, warm gas behind HH shocks typically radiates over an interval from 10 – 100 years after it passes through the shock, and as such is relatively unaffected by short-term variations in the preshock density.

(2) Proper motions generally decline with increasing distance from the jet axis.

(3) There is a correlation between the shock orientation and the observed proper motion. Bow shocks that curve back towards the source tend to have the greatest proper motions. Reverse bow shocks (those which curve away from the source as would be the case for a shock around a stationary or slowly moving obstacle) usually have low proper motions but can exhibit large radial velocities and velocity dispersions (*e.g.* HH 29; Fig. 3).

(4) Large differential motions exist within single bow shock systems. Such motions are often associated with multiple clumps that lie within larger structures that appear to have fragmented. The rapid development of instabilities within shocks and their cooling layers are one way to fragment bow shocks into clumps.

## IV. MOLECULAR EMISSION FROM JETS

Observations of shock-excited $H_2$ emission in outflows provide a crucial link between high velocity, optically visible Herbig-Haro objects and lower velocity molecular outflows. Near-infrared lines, such as the 2.12 $\mu$m S(1) line of $H_2$, probe the physical conditions in shocks with velocities ranging from about 20 km s$^{-1}$ in purely hydrodynamic shocks to over 100 km s$^{-1}$ in magnetized C-shocks where strong magnetic fields cushion the shock and enable $H_2$ molecules to survive higher velocities which would otherwise dissociate molecules (Hollenbach 1997). These

molecular shocks are typically invisible optically, either because the optical emission is intrinsically fainter than the $H_2$ emission in these flows or because the extinction is an order of magnitude higher at optical wavelengths than it is at $2\mu$m.

Examples of obscured YSOs with extensive $H_2$ outflows include the class 0 sources L 1448C (Bally et al 1993; Davis et al 1994a; Davis & Smith 1996a), IC 348-IR (McCaughrean et al. 1994), L 1634-IR (Eislöffel 1997), and IRAS 05413-0104, the source of the spectacular HH 212 outflow in Orion B (Zinnecker et al. 1998). Though portions of these flows are sometimes visible as Herbig-Haro objects, the full morphology only appears in deep $H_2$ images. The $H_2$ emission in these flows traces bow shocks which move into the downstream medium and shocks which propagate back into the jet. $H_2$ emission is also a potent tracer of outflows from high luminosity YSOs ($10^4$ $L_\odot$ – $10^5$ $L_\odot$) that tend to be located in more distant and relatively obscured clouds. Spectacular examples include the fingers of $H_2$ emission associated with the massive OMC1 outflow behind the Orion Nebula (Allen & Burton 1993), and the molecular bubble and jet that emanates from massive young stars in Cepheus A (Hartigan et al. 1996).

Recent important results from studies of shock-excited $H_2$ emission include:

(1) Outflows accompany even the youngest protostars. The vast majority of Class 0 and extreme Class I protostars are associated with outflows and shock systems (Yu et al. 1997; Bontemps et al. 1996). Owing to the large extinction toward these objects, such outflows are best traced with $H_2$ images.

(2) The more highly embedded, younger outflows generally have lower velocities and higher densities than the older Herbig-Haro flows. This behavior may arise because outflows driven by accretion should have terminal velocities comparable to the escape velocities in their acceleration regions. Younger T Tauri stars have relatively larger radii, and correspondingly lower escape velocities.

(3) Outflows from low mass protostars such as the IRAS 05413-0104, the exciting source of HH 212 (Zinnecker et al. 1998), tend to be better collimated and more jet-like than outflows from high mass YSOs such as Cepheus A (Hartigan et al 1996), OMC 1, and DR 21 (Garden et al. 1991).

(4) Shock excited $H_2$ emission can trace sites of momentum transfer between stellar jets and their associated CO outflows. In these cases CO emission surrounds the stellar jet in a sheath-like morphology (Reipurth & Cernicharo 1995; Nagar et al 1996). Molecular emission also sometimes accompanies the wings of high excitation bow shocks (HH 32, Davis et al. 1996a; HH 1, Davis et al. 1994b).

(5) Shock-excited $H_2$ also occurs ahead of some optically visible low-excitation HH bow shocks (*e.g.* HH 7; Carr 1993). This emission

has kinematics and spatial distribution characteristic of a magnetic precursor or a C-shock.

## V. PARSEC-SCALE HH FLOWS

Perhaps the most unexpected result in HH research in recent years has been the realization that jets are not the tiny flows once envisaged, but that they can extend many parsecs. The first parsec-scale Herbig-Haro flow discovered was the HH 34 system located about 1.5° south of the Orion Nebula (Bally & Devine 1994). The outflow consists of a $20'$ long chain of HH objects which corresponds to a projected length of 2.7 parsecs at a distance of 460 pc. Radial-velocity and proper-motion measurements for a number of giant outflow complexes such as HH 34 (Devine et al. 1997) and HH 111 (Reipurth et al. 1997a; Fig. 4) show that all components move away from the central source and decline systematically in radial velocity and proper motion with increasing projected distance from the source. The dynamical ages of these giant flows are $\tau_{dyn} = 10^4\, d_{pc}/v_{100}$ years, where $d$ is the distance from the source in parsecs and $v_{100}$ is the apparent velocity in units of 100 km s$^{-1}$. These ages range from over $10^4$ years to nearly $10^5$ years, comparable to the accretion time for a typical low mass star. Reipurth et al. (1997) discuss over 20 examples of outflows traced by their HH objects with lengths ranging from 1 to over 7 parsecs. Hence, the morphology and distribution of the shocks in an HH flow complex trace the mass loss history from the YSO *over a time scale comparable to its accretion time.*

Most parsec-scale flows consist of more or less regularly spaced HH objects, implying that major outbursts occur every several hundred to a thousand years, comparable to the expected intervals between massive accretion events known as FU Ori outbursts (Reipurth 1989; Hartmann et al. 1993). Though many show S-shaped point reflection symmetry about the central source (Gomez et al. 1997), a few show C-shaped symmetry (Bally et al. 1996a) similar to some extragalactic jets.

Systematic trends in the properties of HH flows depend on the projected separation of the HH objects from their driving sources. HH objects close to their sources often contain highly collimated, fast moving, but low-excitation knots that trace the inner jet. Farther out, HH objects tend to be bow-shaped and exhibit higher excitation line emission. The most distant shocks appear highly fragmented with amorphous morphologies and have lower velocities than HH objects closer to the source. The sizes of HH objects also tend to increase with increasing distance from the driving source, and a few HH bow shocks are nearly 1 parsec in extent (*e.g.* the terminal bow shock HH 401 of the HH 1/2 system; Ogura 1995).

The observed properties of parsec-scale HH flows require several

kinds of mass-loss variability in the source. The periodicity, low excitation, and high proper motions of knots in the inner jets can be explained by a *variable ejection velocity*, while the S-shaped symmetry seen in the extended outflow complexes (cf. HH 34 and HH 315) requires a *variable ejection angle*. The mass-loss rate and possibly the degree of collimation may also be time-dependent.

Many parsec-scale HH flows are larger than their CO counterparts, which tend to have dimensions comparable to the host cloud cores (0.05 to 0.3 pc in CO). It is likely that close to their sources jets entrain CO bearing gas and produce bipolar CO outflows, while farther from the sources jets entrain predominantly atomic gas.

In several parsec-scale HH flows, shock-excited optical emission is seen towards low obscuration regions where galaxies and rich star fields are visible. These outflows have punched out of their parent cloud cores and are pumping energy and momentum into the inter-clump medium of giant molecular clouds or into the surrounding interstellar medium. It may be possible to constrain the nature of the intercloud medium of giant molecular clouds by analyzing the terminal working surfaces of giant HH flows. The low extinction towards the lobes of several of the parsec-scale outflows and the large velocities observed for some flow components imply that UV and X-ray techniques may be used to investigate some outflows from young stars. It may be possible to detect highly ionized species such as O VI, Si III, and C IV either in absorption against bright background stars or, in some cases, directly in emission.

The large number of known HH objects, their high surface area covering factor, and their large angular scales imply that outflows profoundly affect the molecular cloud environment in active star formation regions such as NGC 1333 in Perseus and in Orion (Bally et al. 1996b; Reipurth et al. 1997a). Terminal working surfaces penetrate the cloud volume, blow out of their host cores, shock, dissociate, and even ionize the material they encounter. Outflows may be important in the overall stability of clouds; their shocks may dissociate molecules and be responsible for the large observed abundances of neutral or ionized carbon deduced from sub-millimeter and far infrared observations, and may generate turbulence in molecular clouds, helping to support the clouds against gravitational collapse.

## VI. MULTIPLE JETS AND MULTIPLE SOURCES

Most stars are found in binaries. Recent studies have documented that this is also true for young pre-main sequence stars (e.g. Reipurth & Zinnecker 1993, Ghez et al. 1993). The peak of the separation distribution function for main sequence stars is around 30 AU (Duquennoy & Mayor 1991), which for the nearest star forming regions translates

into sub-arcsecond separations. This is an important fact, because 30 AU is smaller than the typical disk sizes around young stars, and consequently disks are likely to play significant roles in the early evolution of young binaries. One would expect that there are two types of disks among binary systems: circumstellar disks which surround individual binary components, and circumbinary disks that encompass entire binaries. For certain separations it is likely that individual disks orbit individual components, while a circumbinary disk at the same time surrounds the whole binary, with a tidally induced gap between the inner and outer disks (Mathieu 1994; Artymowicz & Lubow 1994).

An increasing number of double jets are being discovered (Reipurth et al. 1993; Gredel & Reipurth 1994), documenting that very young jet sources can have two simultaneously active components. Other evidence for active young binaries come from the discovery of quadrupolar molecular outflows (Avery et al. 1990). HST has recently been used with NICMOS to image jet sources, which are among the youngest stars known. The new images resolve several binaries, in some cases with binary jets emerging at large projected angles to one another (Reipurth et al. 1998b). If we assume that a jet is launched perpendicular to its accretion disk (a likely assumption, but proven in only a few cases thus far; *e.g.* Ohashi & Hayashi 1996) then these observations imply that the circumstellar accretion disks may not be co-planar. The episodic behavior of binary jets may provide clues about mutual disk interactions and the fueling of circumstellar disks from circumbinary disks.

Figure 5 shows a recent HST NICMOS observation at 1.6 $\mu$m of the HH 1 jet, which demonstrates that another flow emanates from a cavity near the embedded HH 1 source. A third flow source (located just outside the figure) is deeply embedded and is seen only at cm wavelengths; the three sources together are likely to form a non-hierarchical triple system, in which strong tidal forces must act and vary on orbital time scales. Such time scales are mostly short compared to the duration of outflow activity, and therefore jet axes should be affected by precession. Jets may therefore carry information on the orbital history of very young binaries. A recently discovered case in which binary motion may influence the ejection direction of one of the lobes of a binary jet is the outflow from the T Tauri star Haro 6-10 (Devine et al. 1998).

## VII. JETS WITHIN H II REGIONS

One of the difficulties in studying stellar jets and HH objects is that we only see the portion of the flow that cools after passing through shocks. However, if the jet lies within an H II region, then all of the gas in the flow can become visible because, depending on its density, the jet may be fully photoionized. The advantage of being able to observe the entire outflow is reduced somewhat by the difficulty in distinguishing

the jet from the ambient gas, though flows can be identified in this manner through Fabry-Perot spectroscopy (O'Dell et al. 1997a). Emission line ratios are more complex in these regions because the excitation is a mix of photoionization and shock heating, and the preshock ionization is affected by the ultraviolet light which ionizes the H II region. As for normal bow shocks (section III), a bow shock within an H II region should have its highest excitation lines at the apex. This was indeed found to be the case for most of the HH objects studied by HST within the Orion Nebula (O'Dell et al. 1997b). When the bow shock is not illuminated uniformly by ambient ultraviolet light, as occurs within HH 203/204 in Orion, the line excitation maps show a more complex morphology (Fig. 6).

We are currently identifying a group of young stellar objects for which it will be possible to study the kinematics of jets close to the star, where the jets become collimated (Reipurth et al. 1998a). These jets lie within a H II regions, so much of the gas within them is heated by photoionization, and can be distinguished from the rest of the nebular gas by its Doppler motion. Surprisingly, only one side of the jet has been found in many of these sources. Similar objects exists in the outskirts of the Orion Nebula and near the NGC 1333 reflection nebula that is illuminated by a B star. All indications are that these irradiated jets are common, but they simply have escaped detection up to now because they are embedded in bright HII regions or reflection nebulae.

## VIII. CONCLUDING REMARKS

The wealth of new observations of Herbig-Haro jets discussed in this chapter make it clear that these flows play a significant role in the star formation process, both close to the star where the accretion disk loses angular momentum and accelerates the jet in sudden accretion events, and far from the star as the jet transfers its energy to the surrounding molecular cloud. To a large extent, conditions within HH flows are determined by events which occurred close to the young star in the recent past, and, when read properly, HH flows provide a unique record of this past.

A number of exciting developments should occur in the study of HH jets in the immediate future. As the number of jets observed and reobserved with HST increases, we can expect a series of spectacular movies of HH motion that can be compared directly to similar numerical simulations. Such data will undoubtedly revolutionize the field in unexpected ways. Additional spectroscopy and images over large fields of view will continue to clarify which dynamical processes are important in HH flows. Many of the basics of HH dynamics, particularly the roles of magnetic fields and molecular cooling in the flows, remain uncertain at this point. Finally, studies of binary jets and of flows within

H II regions alluded to in this chapter have great promise in opening new avenues of research. We have just begun to appreciate the major effect stellar jets have on the dynamics and morphologies of molecular clouds, the intercloud medium, and future sites of star formation.

## REFERENCES


Allen, D., & Burton, M. 1993, *Nature* 363:54–56.

Artymowicz, P. & Lubow, S.H. 1994, *Astrophys. J.* 421:651–667.

Avery, L.W., Hayashi, S.S., White, G.J. 1990, *Astrophys. J.* 357:524–530.

Bachiller, R. 1996, *Ann. Rev. Astron. Astrophys.* 34:111–154.

Bally, J., & Devine, D. 1994, *Astrophys. J.* 428:L65–L68.

Bally, J., Devine, D., & Alten, V. 1996a, *Astrophys. J.* 473:921–928.

Bally, J., Devine, D., Reipurth, B. 1996b, *Astrophys. J.* 473:L49–L52.

Bally, J., Lada, E., & Lane, A. 1993, *Astrophys. J.* 418:322–327.

Beck-Winchatz, B., Böhm, K.H., and Noriega-Crespo, A. 1996, *Astron. J.* 111:346–354.

Blondin, J., Königl, A., & Fryxell, B. 1990, *Astrophys. J.* 360:370–386.

Bontemps, S., Andre, P., Tereby, S., & Castets, S. 1996, *Astron. Astrophys.* 311:858–872.

Bouvier, J., Cabrit, S., Fenandez M., Martin, E., Matthews, J. 1993, *Astron. Astrophys. Suppl.* 101:485–498.

Burrows, C. J. et al. 1996, *Astrophys. J.* 473:437–451.

Carr, J. 1993, *Astrophys. J.* 406:553–562.

Cernicharo, J., & Reipurth, B. 1996, *Astrophys. J.* 460:L57–L60

Chernin, L., & Masson, C. 1995, *Astrophys. J.* 455:182–189.

Chevalier, R., & Raymond, J. 1978, *Astrophys. J.* 225:L27–L30.

Chevalier, R., Kirchner, R. & Raymond, J. 1980, *Astrophys. J.* 235:186–195.

Cioffi, D. F., & Blondin, J. 1992, *Astrophys. J.* 392:458–464.

Cox, D., & Raymond, J. 1985, *Astrophys. J.*, 298:651–659.

Davis, C., Dent, H., Matthews, H., Aspin, C., & Lightfoot, J. 1994a, *Mon. Not. Roy. Astron. Soc.* 266:933–944.

Davis, C., Eislöffel, J., & Ray, T. 1994b, *Astrophys. J.* 426:L93–L95.

Davis, C. & Eislöffel, J. 1995, *Astron. Astrophys.* 300:851–869.

Davis, C. & Smith, M. 1996a, *Astron. Astrophys.* 309:929–938.

Davis, C. & Smith, M. 1996b, *Astron. Astrophys.* 310:961–969.

Davis, C., Eislöffel, J., & Smith, M. *Astrophys. J.* 463:246–253.

Devine, D., Bally, J., Reipurth, B., & Heathcote, S. 1997, *Astron. J.* 114:2095–2111.

Devine, D., Reipurth, B., Bally, J., & Balonek, T. 1998, *Astron. J.* in press.

DeYoung, D. 1986, *Astrophys. J.* 307:62–72.

Dopita, G. 1995, Photoionizing Shocks. In *The Analysis of Emission*

*Lines*, eds. R. E. Williams & M. Livio, (Cambridge: Cambridge University Press), pp. 65–82.
Draine, B. 1980, *Astrophys. J.* 241:1021–1038.
Draine, B., & McKee, C. 1993, *Ann. Rev. Astron. Astrophys.* 31:373–432.
Duquennoy, A., & Mayor, M. 1991, *Astron. Astrophys.* 248:485–524.
Edwards, S. et al. 1993, *Astron. J.* 106:372–382.
Eislöffel, J., & Mundt, R. 1997, *Astron. J.* 114:280–287.
Eislöffel, J. 1997, Molecular Hydrogen Emission in Embedded Flows. In *Herbig-Haro Flows and the Birth of Low Mass Stars*, I.A.U. Symposium No. 182, B. Reipurth & C. Bertout eds., (Dordrecht: Kluwer), pp 93–102.
Ferland, G. 1995, The Lexington Benchmarks for Numerical Simulations of Nebulae. In *The Analysis of Emission Lines*, eds. R. E. Williams & M. Livio, (Cambridge: Cambridge University Press), pp. 83–96.
Fridlund, C.V.M., Liseau, R., & Gullbring, E. 1998, *Astron. Astrophys.* 330:327–335.
Garden, R., Geballe, T., Gatley, I., & Nadeau, D. 1991, *Astrophys. J.* 366:474–483.
Ghez, A.M., Neugebauer, G., Matthews, K. 1993, *Astron. J.* 106:2005–2023.
Gomez, M., Kenyon, S., & Whitney, B. 1997, *Astron. J.* 114:265–271.
Gredel, R., Reipurth, B. 1993, *Astrophys. J.* 407:L29–L32.
Gredel, R., Reipurth, B. 1994, *Astron. Astrophys.* 289:L19–L22.
Hartigan, P. 1989, *Astrophys. J.* 339:987–999.
Hartigan, P. 1997, HST Observations of the HH 47 and HH 111 Stellar Jets. In *Accretion Phenomena and Related Outflows*, IAU Colloquium 163, ASP Conference Series Vol. 121, D. T. Wickramasinghe, G. V. Bicknell, & L. Ferrario eds., pp. 536–545.
Hartigan, P., Carpenter, J., Dougados, C., & Skrutskie, M. 1996, *Astron. J.* 111:1278–1285.
Hartigan, P., Edwards, S., & Ghandour, L. 1995, *Astrophys. J.* 452:736–768.
Hartigan, P., Morse, J., Heathcote, S., Cecil, G., & Raymond, J. 1993, *Astrophys. J.* 414:L121–L124.
Hartigan, P., Morse, J., & Raymond, J. 1994, *Astrophys. J.* 436:125–143.
Hartigan, P., Morse, J., Tumlinson, J., Raymond, J., & Heathcote, S. 1998, *Astrophys. J.* in press.
Hartigan, P., Raymond, J., & Hartmann, L. 1987, *Astrophys. J.* 316:323–348.
Hartigan, P., Raymond, J., & Meaburn, J. 1990, *Astrophys. J.* 362:624–633.
Hartmann, L., Kenyon, S., & Hartigan, P. 1993, Young Stars: Episodic

Phenomena, Activity and Variability. In *Protostars & Planets III*, eds. E. H. Levy and J. I. Lunine (Tucson: Univ. of Arizona Press), pp. 497–518.

Heathcote, S., Morse, J., Hartigan, P., Reipurth, B., Schwartz, R.D., Bally, J., & Stone, J. 1996, *Astron. J.* 112:1141–1168.

Heathcote, S., & Reipurth, B. 1992, *Astron. J.* 104:2193–2212.

Heiles, C., Goodman, A., McKee, C., & Zweibel, E. 1993, Magnetic Fields In Star-Forming Regions: Observations. In *Protostars & Planets III*, eds. E. H. Levy and J. I. Lunine (Tucson: Univ. of Arizona Press), pp. 279–326.

Herbig, G. & Jones, B. 1981, *Astron. J.* 86:1232-1244.

Hester, J., Stapelfeldt, K., & Scowen, P. 1998, *Astron. J.* 116:372–395.

Hollenbach, D. 1985, *Icarus* 61:36–39.

Hollenbach, D. 1997, The Physics of Molecular Shocks in YSO Outflows. In *Herbig-Haro Flows and the Birth of Low Mass Stars*, I.A.U. Symposium No. 182, B. Reipurth & C. Bertout eds., (Dordrecht: Kluwer) pp. 181–198.

Lavalley, C., Cabrit, S., Dougados, C., Ferruit, P., & Bacon, R. 1997, *Astron. Astrophys.* 327:671–680.

Livio, M. 1997, The Formation of Astrophysical Jets. In *Accretion Phenomena and Related Outflows*, I.A.U. Colloquium 163, eds. D. T. Wickramasinghe, G. V. Bicknell, & L. Ferrario (San Francisco: ASP Publications), pp. 845–866.

Mathieu, R.D. 1994, *Ann. Rev. Astron. Astrophys.* 32:465–530.

McCaughrean, M., Rayner, & Zinnecker, H. 1994, *Astrophys. J.* 436:L189–L192.

Moriarty-Schieven, G. H., Butner, H. M., & Wannier, P. G. 1995, *Astrophys. J.* 445:L55–L58.

Morse, J., Hartigan, P., Cecil, J., Raymond, J., & Heathcote, S. 1992, *Astrophys. J.* 399:231–245.

Morse, J., Hartigan, P., Heathcote, S., Raymond, J., & Cecil, G. 1994, *Astrophys. J.* 425:738–754.

Morse, J., Heathcote, S., Cecil, G., Hartigan, P., & Raymond, J. 1993, *Astrophys. J.* 410:764–776.

Nagar, N. M., Vogel, S., Stone, J., & Ostriker, E. 1997, *Astrophys. J.* 482:L195–L198.

Najita, J., & Shu, F. 1994, *Astrophys. J.* 429:808–825.

Noriega-Crespo, A., Garnavich, P., Raga, A., Canto, J., & Böhm, K.-H. 1996, *Astrophys. J.* 462:804–812.

Norman, M. L., Smarr, L. L., Winkler, K.-H., & Smith, M. 1982, *Astron. Astrophys.* 113:285–302.

Morse, J., et al. 1996, *Publ. Astron. Soc. Pacific* 108:426–440.

O'Dell, C. R., Hartigan, P., Bally, J., & Morse, J. 1997a, *Astron. J.* 114:2016–2028.

O'Dell, C. R., Hartigan, P., Lane, W. M., Wong, S. K., Burton, M. G.,

Raymond, J., & Axon, D. J. 1997b, *Astron. J.* 114:730–743.
Ohashi, N., & Hayashi, M. 1996, High Resolution Observations of Disks Around Protostellar Sources with the Nobeyama Millimeter Array. In *Disks and Outflows Around Young Stars*, S. Beckwith et al. eds., (Berlin: Springer-Verlag), pp. 44–57.
Ogura, K. 1995, *Astrophys. J.* 450:L23–L26.
Osterbrock, D. 1989, *Astrophysics of Gaseous Nebulae and Active Galactic Nuclei*, (Mill Valley CA: University Science Books), p. 73.
Raga, A. 1991, *Astron. J.* 101:1472–1475.
Raga, A., et al. 1995, *Rev. Mex. Astron. Astrophys.* 31:51–61.
Raga, A., & Böhm, K.-H. 1986, *Astrophys. J.* 308:829–835.
Raga, A., & Cabrit, S. 1993, *Astron. Astrophys.* 278:267–278.
Ray, T., Mundt, R., Dyson, J. E., Falle, S. A. E. G., & Raga, A. 1996, *Astrophys. J.* 468:L103–L106.
Raymond, J. 1979, *Astrophys. J. Suppl.* 39:1–27.
Raymond, J., Morse, J., Hartigan, P., Curiel, S., & Heathcote, S. 1994, *Astrophys. J.* 434:232–236.
Reipurth, B. 1989, *Nature* 340:42–45.
Reipurth, B., Bally, J., & Devine, D. 1997a, *Astron. J.* 114:2708–2735.
Reipurth, B., Bally, J., Fesen, & Devine, D. 1998a, *Astrophys. J.* in press.
Reipurth, B. & Bertout, C. 1997, *Herbig-Haro Flows and the Birth of Low Mass Stars*, I.A.U. Symposium No. 182, B. Reipurth & C. Bertout eds., (Dordrecht: Kluwer).
Reipurth, B., & Cernicharo, J. 1995, *Rev. Mex. Astron. Astrophys.* Serie de Conferencias 1:43–58.
Reipurth, B., Hartigan, P., Heathcote, S., Morse, J.A., & Bally, J. 1997b, *Astron. J.* 114:757–780.
Reipurth, B. & Heathcote, S. 1992, *Astron. Astrophys.* 257:693–700.
Reipurth, B., Heathcote, S., Roth, M., Noriega-Crespo, A., Raga, A.C. 1993, *Astrophys. J.* 408:L49–L52.
Reipurth, B. & Olberg, M. 1991, *Astron. Astrophys.* 246:535–550.
Reipurth, B., Raga, A., & Heathcote, S. 1996, *Astron. Astrophys.* 311:989–996.
Reipurth, B., Yu, K.C., Bally, J., Rodriguez, L.F. 1998b in preparation.
Reipurth, B., Zinnecker, H. 1993, *Astron. Astrophys.* 278:81–108.
Schwartz, R. D. 1975, *Astrophys. J.* 195:631–642.
Schwartz, R. D. 1981, *Astrophys. J.* 243:197–203.
Shull, J., & McKee, C. 1979, *Astrophys. J.* 227:131–149.
Solf, J. 1987, *Astron. Astrophys.* 184:322–328.
Solf, J., Böhm, K.-H., & Raga, A. 1986, *Astrophys. J.* 305:795–804.
Stone, J., & Norman, M. 1993, *Astrophys. J.* 413:210–220.
Sutherland et al. 1993, *Astrophys. J.* 414:510–526.
Tamura, M., Ohashi, N., Hirano, N., Itoh, Y., & Moriarty-Schieven, G. H. 1996, *Astron. J.* 112:2076–2085.

Yu, K., Bally, J., & Devine, D. 1997, *Astrophys. J.* 485:L45–L48.

Zel'dovich, Y. B., & Razier, Y. P. 1966, *Physics of Shock Waves and High-Temperature Hydrodynamic Phenomena*, (New York: Academic Press), p. 45.

Zinnecker, H., McCaughrean, M., & Rayner, J. 1998, *Nature* 394, 862–864.

## FIGURE CAPTIONS

Figure 1. The structure of a radiative shock. Material enters the shock front at left with a velocity V and is slowed by a factor of 4 after crossing the shock. The density jumps by a factor of 4 at the shock and increases gradually as the gas cools and slows. As an example, cooling zones of oxygen are depicted by the x's, circles and dots. This diagram is drawn in the frame of reference of the shock – for HH objects viewed from the star all components of this diagram would appear to move to the right at a velocity 10V – 20V.

Figure 2. H$\alpha$ arcs and bow shocks within the HH 111 jet from Reipurth et al. (1997b). Left: The inner portion of the jet appears in this image formed from the difference of an H$\alpha$ image and a [S II] image. White areas have stronger [S II] emission than H$\alpha$, and black areas are relatively stronger at H$\alpha$. H$\alpha$ is especially strong in arcs that mark the location of bow shocks in the flow. Middle: Wings of bow shocks are visible to the side of the jet in this H$\alpha$ image. These protruding wings are fainter than the main H$\alpha$ knot in the jet, and indicate that the density exterior to the main part of the jet is low; *i.e.*, the surrounding material does not confine the flow. Right: A series of nested bow shocks makes up the middle portion of the HH 111 jet.

Figure 3. The velocity field of the L 1551 jet and HH 29 obtained from Fabry-Perot data. The R, G, and B labels refer to the velocities of the emission, in $\mathrm{km\,s^{-1}}$ with respect to the molecular cloud, that are loaded into the red, green, and blue channels, respectively for display. Hence, areas in white have emission in each of the channels, and denote ares of large line widths. Top: The jet emerges from an infrared source located above the top of the frame in these images of the L 1551 jet. The highest blueshifted radial velocities occur in the jet, while the bright knot at the end of the jet has a large line width (color white), and is surrounded by a shell of lower velocity material, as expected for a bow shock. Bottom: The bow shock visible in the H$\alpha$ image of HH 29 (left) appears to have wrapped around two of the slowest knots as indicated by the red and green colors in the [S II] image (right).

Figure 4. A composite H$\alpha$ + [S II] image showing the 7 parsec long outflow associated with the HH 111 jet. The upper (left) panel is a mosaic of two CTIO Curtis Schmidt CCD images showing the nearly $1^o$ long Herbig-Haro flow. The middle frame (right) shows an Hubble Space Telescope image of the HH 111 jet. The lower-left (bottom-right) and lower-right (top-right) frames show CCD images of HH 113 and HH 311 at the far ends of the flow obtained with the ESO NTT. Superimposed vectors show the proper motions of the brightest knots. See Reipurth et al. (1997b, 1998a) for details.

Figure 5. An infrared image obtained with the NICMOS camera onboard the Hubble Space Telescope at a wavelength of 1.6 $\mu$m showing the region around the energy source of the HH 1/2 jet. The primary jet is clearly visible in [Fe II] emission all the way to the location of the embedded VLA source. An arc-shaped reflection nebula at lower left opens up towards

a secondary HH flow. Hence, a companion to the VLA source must be located near the apex of the nebula. The two flow axes are indicated. The scale bar of $2''$ corresponds to $\sim$ 920 AU at the distance to these jets. Adapted from Reipurth et al. (1998b).

Figure 6. HST images of the HH 203/204 complex from O'Dell et al. (1997a). The HH objects seem to mark the apices of bow shocks that move to the lower left in the figure. Unlike normal HH objects where the highest ionization lines occur near the apices of bow shocks, in this case the high-ionization line [O III] $\lambda$5007 emits at the right and top of the figure, in the direction of the ionizing source $\Theta_1$C. This region shows an example of a mixture of photoionization and shock excitation.

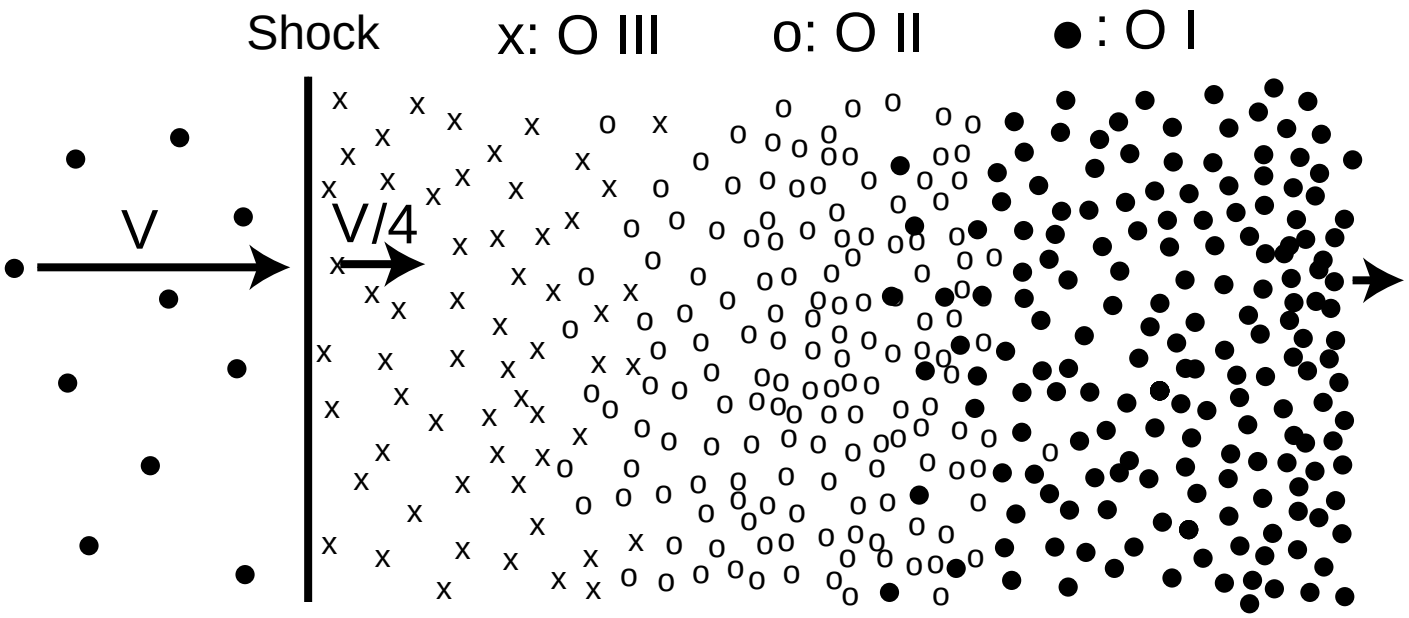
Shock
x: O III
o: O II
● : O I
V
V/4

Bright Faint

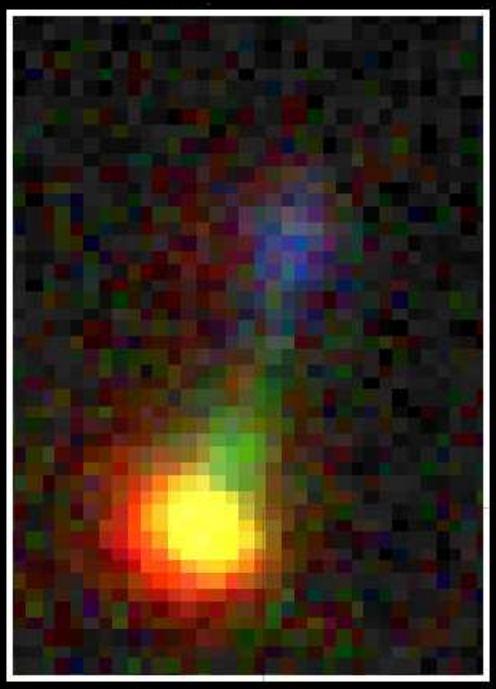

R: - 120, - 150
G: - 180, - 210
B: - 240, - 270

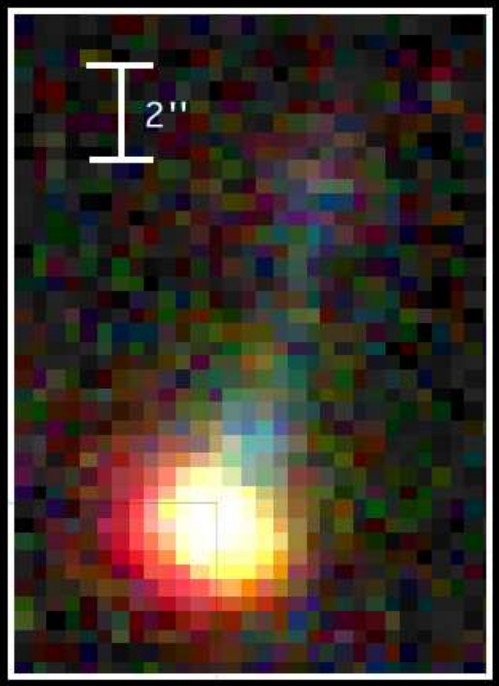


R: - 150
G: - 180
B: - 210

# L1551 Jet

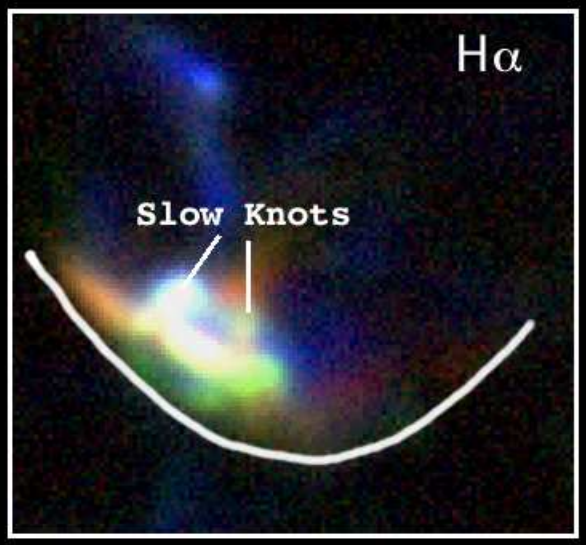


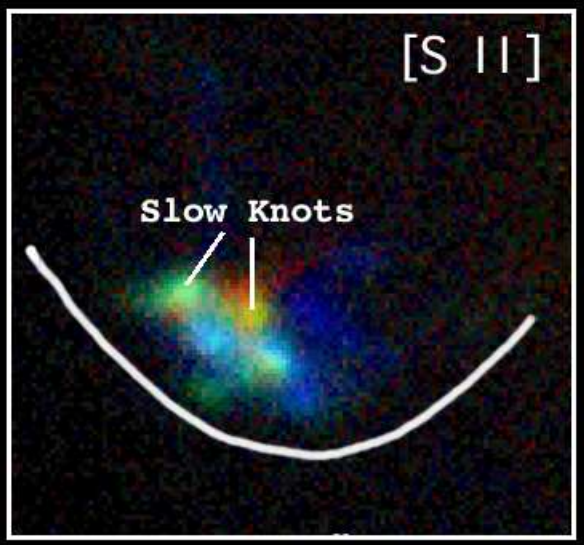


R: +30, 0
G: - 30, - 60
B: - 90, - 120

R: +60, +30, 0, - 30
G: - 60, - 90, - 120
B: - 150, - 180, - 210

# HH 29

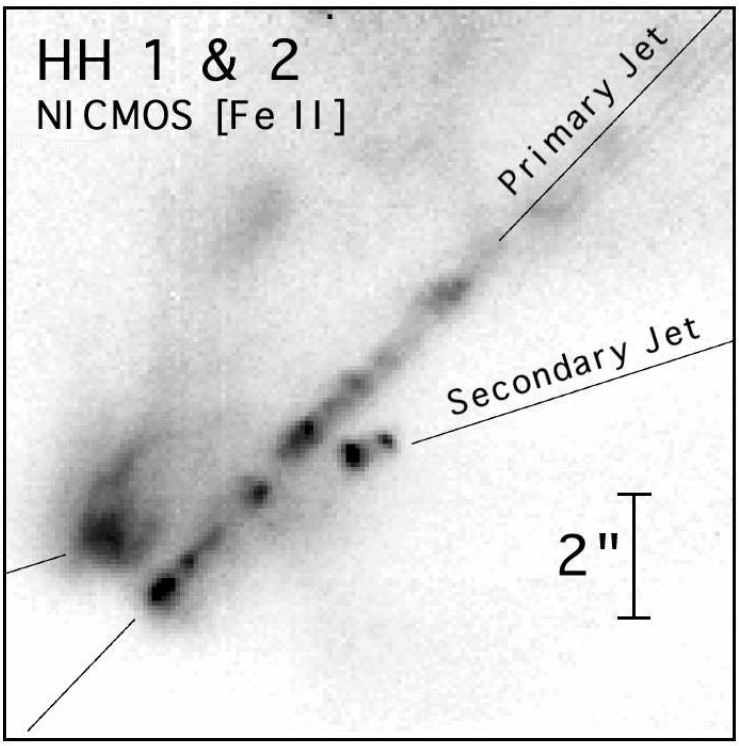
HH 1 & 2
NICMOS [Fe II]
Primary Jet
Secondary Jet
2"

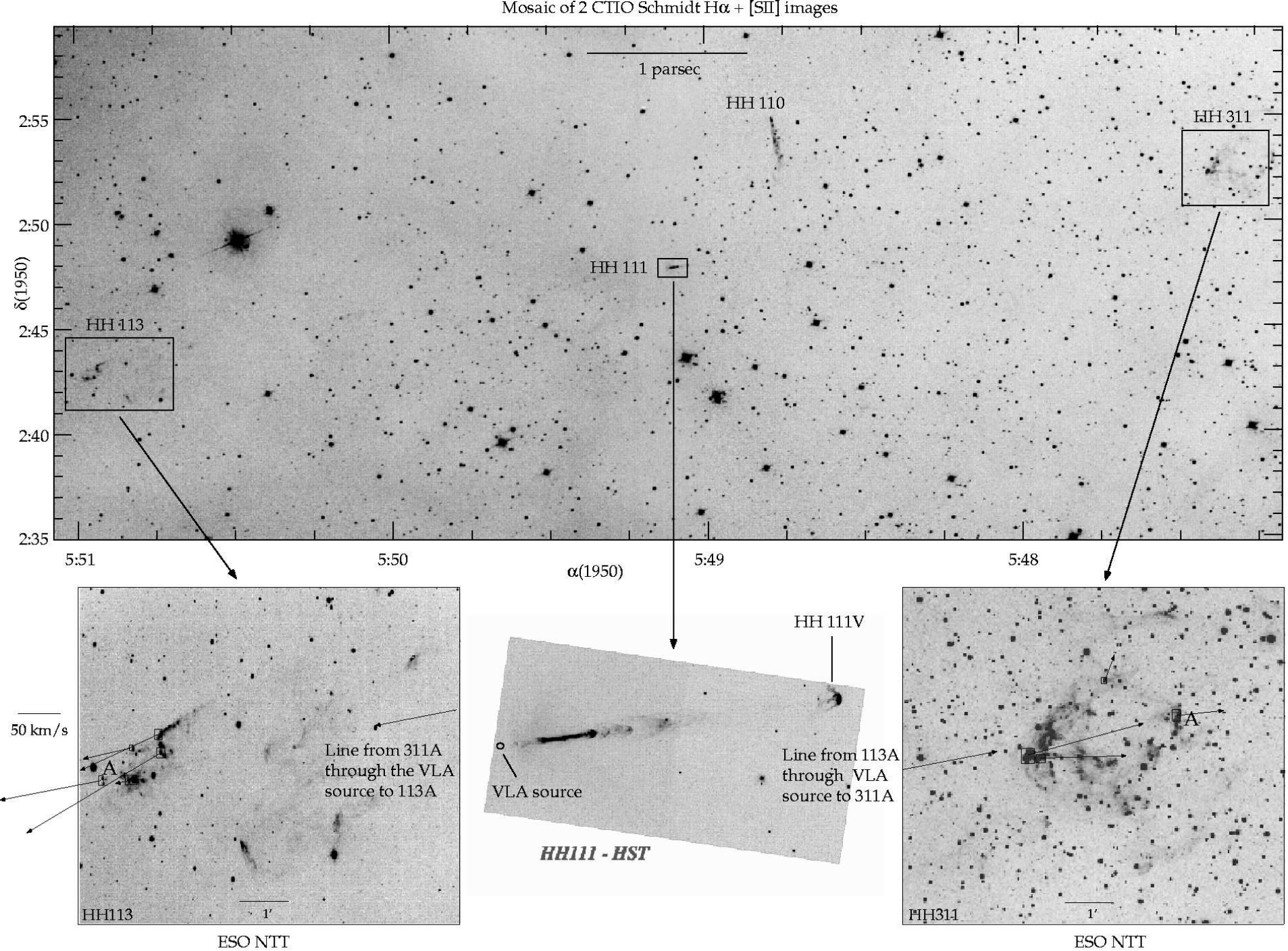
Mosaic of 2 CTIO Schmidt Hα + [SII] images
1 parsec
HH 110
HH 311
HH 111
HH 113
2:55
2:50
2:45
2:40
2:35
δ(1950)
5:51
5:50
5:49
5:48
α(1950)
HH 111V
50 km/s
A
Line from 311A
through the VLA
source to 113A
VLA source
HH111 - HST
Line from 113A
through VLA
source to 311A
A
HH113
1'
HH311
1'
ESO NTT
ESO NTT

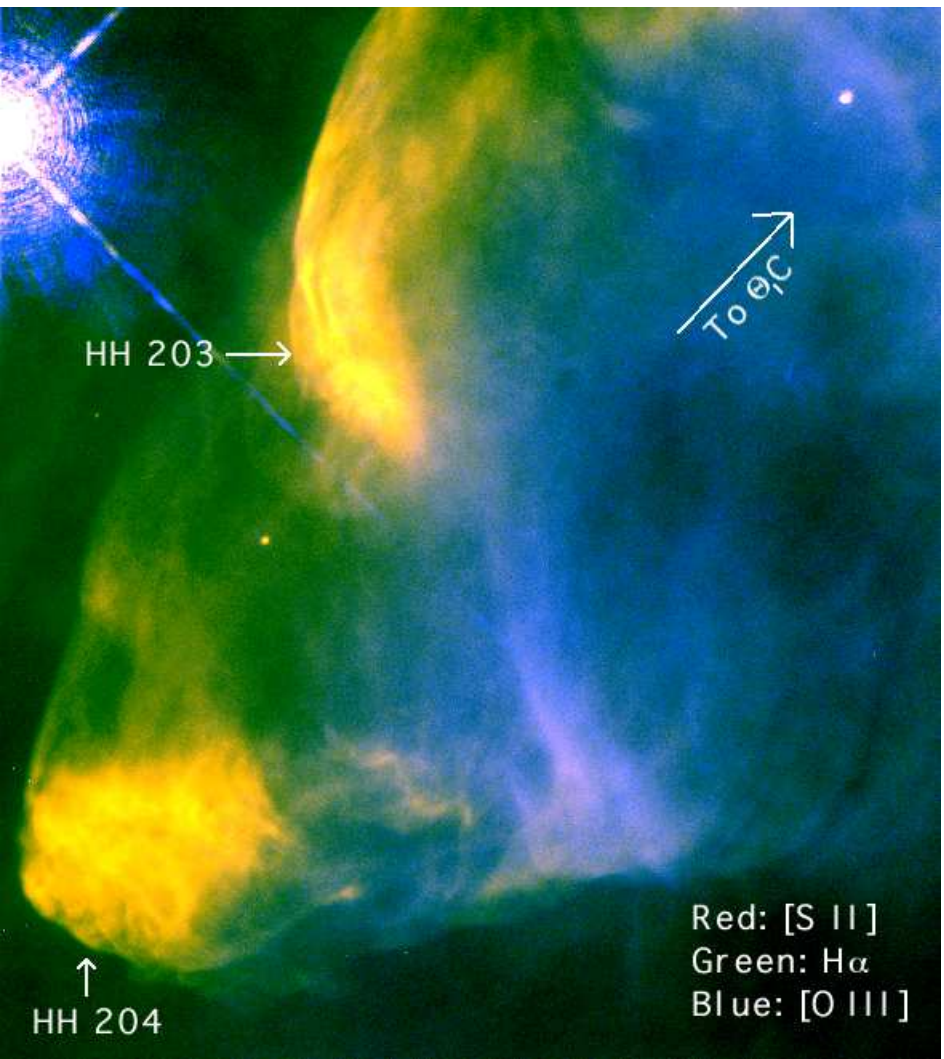
HH 203
To θ¹C
HH 204
Red: [S II]
Green: Hα
Blue: [O III]